RESEARCH ARTICLE

Synthesis of reduced graphene oxide/ZnO nanocomposites using grape fruit extract and *Eichhornia crassipes* leaf extract and a comparative study of their photocatalytic property in degrading Rhodamine B dye

Subramanian Ramanathan[1] · Steplin Paul Selvin[2] · Asir Obadiah[1] · Arulappan Durairaj[1] ·
Palanisamy Santhoshkumar[1] · Sharmila Lydia[2] · Subramaian Ramasundaram[3] · Samuel Vasanthkumar[1]

Abstract
In the present work, we report the comparative study of photocatalytic degradation of Rhodamine B (RhB) dye in aqueous solution by using ZnO-graphene nanaocomposites obtained using two different natural reducing agents namely Grape and *Eichhornia crassipes*. Graphene oxide (GO) was synthesized by Hummer's method followed by reduction of the graphene oxide using natural reducing agents Grape and *Eichhornia crassipes*. The two samples of graphene oxide (Gr-rGO and Ei-rGO) were treated with ZnO to form a rGO-ZnO nanocomposites. The dye degradation was observed by the decrease in the absorption and decolorization in the presence of visible light. The degradation efficiency was found to be dependent on the concentration of rGO-ZnO nanocomposites added to the dye solution. The Ei-rGO has a higher adsorbing capacity due to its large surface area. A degradation efficiency of 67% was achieved by ZnO alone, whereas with the rGO-ZnO nanocomposite, the photocatalytic degradation efficiency for removal of RhB dye was found to be enhanced. The degradation efficiency was 70.0% and 97.5% with Gr-rGO-ZnO and Ei-rGO-ZnO nanocomposites respectively. The enhanced photocatalytic activity of Ei-rGO-ZnO composites could be attributed to the strong interaction with the ZnO and the defect sites available in Ei-rGO.

Highlights • Use of eco-friendly reducing agents like grapes and *Eichhornia crassipes* for preparation of two varieties of rGO.
• Nanocomposites prepared using ZnO with the two varieties of rGO.
• Degradation efficiency of the two nanocomposites studied under visible light condition on Rhodamine B dye.
• Nanocomposites obtained from the *Eichhornia crassipes* reduction of GO has better degradation efficiency.

✉ Samuel Vasanthkumar
   kumar2359@yahoo.com

1   Department of Chemistry, Faculty of Chemistry, Karunya University, 641114 Coimbatore, India

2   Department of Chemistry, Bishop Heber College, Tiruchirappalli 620017, India

3   Regional Innovation Center for Printed Electronics, Sunchon National University, Sunchon, Jeonnam, Republic of Korea

Introduction

Dyes are organic compounds which are used to colour fibers. Dye can be classified as natural and synthetic. Synthetic dyes are manmade dyes, obtained from resources like petroleum by product, earth minerals and various chemicals. Synthetic dyes are most commonly used in textile industries, due to their color flexibility and improved fastness [1, 2]. Textiles industries use synthetic dyes in large quantities and the dye effluent from these dye houses pose many of environmental problems [3–5]. Removal of dye from dye house effluents by degradation has been actively pursued by many re-searchers as dyes are carcinogenic [6–9]. Untreated dye effluent, can cause lots of damage to water bodies. The contaminated water is unfit for human

consumption. It causes lots of harmful health issues to human beings such as cancer, dermatitis, respiratory diseases, allergic reaction in eyes, skin irritation, and irritation to mucus membrane and the upper respiratory tract. [10–13].

Waste water management is essential to tackle these health problems. Many methods are reported in literature for waste water treatment. Some of the methods are chlorination [14], adsorption [15, 16] carbon filtering [17], desalination [18], distillation [19], electrode ionization [20], etc., Apart from these methods photocatalytic treatment is a well-established technique for pollutant degradation in dye effluents [21]. Photocatalysis involves the passage of light onto a semiconductor oxide/sulphide layer resulting in movement of electrons from the valance band to the conductance band. Superoxide anions and hydroxide radicals which have potential oxidizing and reducing abilities are generated by the photocatalytic setup when the electron hole pairs developed react with the oxygen and water molecules [22].

In recent studies, a semiconductor in combination with some other materials to form a composite for better photocatalytic functioning has been employed [23, 24]. In this work, we have used reduced GO and ZnO composite as photocatalyst for the photocalatytic degradation of RhB dye. The rGO is a thin layer of pure carbon and it is a single, tightly packed layer of both carbon atoms that are bonded together in a hexagonal honeycomb lattice. [25]. It is a good conductor of heat at room temperature and electricity [26]. The synthesis of rGO employing eco-friendly approach is a prominent methodology for research among the scientists. It has a huge number of applications in supercapacitors [27], batteries [28], transistors [29], solar cells [30] and sensors [31]. The production of reduced graphene oxide is carried out by many methods such as electrochemical reduction [32], reduction of GO by hydrazine [33], reduction of GO by thiourea [34], reduction of GO by sodium borohydride [35], reduction of GO via bacterial respiration [36], reduction of GO via l-ascorbic acid [37], reduction of GO by hydrazine hydrate [38] and thermal reduction of GO [39]. These known methods of reduction that employ the usage of chemical reducing agents are toxic in nature, harmful to the environment and lead to the formation of irreversible agglomerates that cause surface modification of the GO [40]. These considerations led us to develop a cost effective and eco- friendly method for the reduction of GO to rGO using fresh grapes and *Eichhornia crassipes* leaf extract as a reducing agent. The reduced GO was derived using two different natural reducing agents Grape and *Eichhornia crassipes* and their performances have been compared.

Experimental

Materials

Graphite powder, ethanol, hydrazine mono hydrate, potassium permanganate, sulphuric acid, hydrochloric acid, and hydrogen peroxide purchased from Merck, Steinem, Germany were used in this study. Grape was purchased from the local market in Karunya nagar, Coimbatore, South India. The Plant *Eichhornia crassipes (mart.) Solms -Laub*.was collected from the Ukkadam pond, Coimbatore, South India. This plant was identified and certified (BSI/SRC/5/23/2011–12/Tech-145) by Botanical Survey of India, Coimbatore. The specimen of the plant was stored in the herbarium (Acc.No. 006149) of Bharathiar University, Coimbatore.

Synthesis of GO

Graphene Oxide was synthesized using the Modified Hummer's method [41]. In this method, graphite flakes were dissolved in concentrated sulphuric acid at 0-5 °C. After a few minutes sodium nitrate solution was mixed with the graphite solution and stirred continuously for 2 h. Then, potassium permanganate (0.5 mol) was added in regular intervals of time (half an hour). After the addition of $KMnO_4$ a pasty brownish product was formed, and it was stirred for 2 days. After stirring, the solution was diluted with water and treated with 30% H_2O_2 (10 ml). The product became yellow in colour. Then it was washed with 10% HCl and water, filtered and dried to get the powder form of Graphene Oxide.

Plant extract preparation

Fresh grapes (*Vitis vinifera*) and *Eichhornia crassipes* leaf were collected from the Western Ghats forest around Coimbatore region of South India. The fresh grapes and *Eichhornia crassipes* leaf were washed thoroughly to remove debris from its parts. The fresh clean parts of grapes and *Eichhornia crassipes* leaf were cut into small pieces and dried at 40 °C in N_2 atm for a few days. The dried parts were taken in a Soxhlet apparatus and using ethanol as the solvent, the Soxhlet extraction was carried out. The extract was collected and the solvent was removed using a Rotary evaporator (Equitron). The aqueous extract was dried and filtered using a Whatman filter paper (0.1 μm in pore size).

Synthesis of rGO

Two varieties of rGO were synthesized, using natural reducing agents like Grape and *Eichhornia crassipes* [42, 43]. 40 ml of

the dispersed Graphene Oxide was obtained by sonication and 30 ml of Grape extract and 30 ml of *Eichhornia crassipes* extracts were obtained by the soxhlet method. Graphene oxide solution was treated with these two extracts separately in a separate round bottom flask and it was refluxed at 80 °C for 5 h. The colour of the solution changed after 5 h from brown to black, indicating the reduction of Graphene Oxide by the natural reducing agents and the product was filtered and dried to get the powder form of r-GO,which was characterized.

Preparation of ZnO/rGO nanocomposites

Ei-rGO-ZnO and Gr-rGO-ZnO nanocomposites were prepared by following the chemical precipitation method. 0.1 M Zinc acetate dihydrate with calculated (0.05 g) amount of corresponding rGO was stirred magnetically for 30 min at 80 °C. To this 0.2 M NaOH solution was added and stirred continuously for 3 h. Finally, the precipitate was washed a number of times with water and ethanol. The resultant product Ei-rGO-ZnO and Gr-rGO-ZnO were dried in an oven at 80 °C for 4 h. Likewise, pure ZnO nanoparticles were prepared by the above mentioned method without the addition of rGO [44].

Photocatalytic experiment

The photocatalytic activity of rGO-ZnO nanocomposite was evaluated by inspecting the photo degradation of RhB as a model pollutant under visible-light irradiation using a 70 W CFL lamp ($\lambda > 400$ nm 70 WBCB22 220–240 V Philips India). In a typical procedure, calculated amount of the synthesized nanocomposite was dispersed in a 100 ml cylindrical vessel. The aqueous solution of the organic dye was prepared in 1×10^{-5} M concentration. Prior to irradiation, the mixture was magnetically stirred for 10 min in the dark to allow adsorption-desorption equilibrium of RhB on the surface of the photocatalyst. After that, the dye solution was irradiated with light using a 70 W CFL lamp. At regular time intervals, 3 ml aliquots were withdrawn and the concentration of the sample was analyzed using a UV-Visble spectrophotometer. The percentage of decolourisation of RhB was calculated using the equation

$$\%D = (A_0 - A_t) \, x100/A_0 \quad (1)$$

Where, A_0 is the initial concentration and A_t is the equilibrium concentration at time 't'.

Characterization

The Fourier transform infrared spectroscopy (FT-IR) was used for IR characterization in the range 4000–400 cm^{-1}

using a Shimadzu FT-IR (Japan) spectrophotometer. The X-ray diffraction studies were performed using a Shimadzu XRD 6000 (Japan) equipment. SEM (JEOL-ASM 6390 (Japan)) and TEM (JEM 2100) techniques were used for surface morphology studies. UV-Visible spectrophotometer (Jasco V-630, Japan) was employed for absorption spectral studies and a Shimadzu (DTG-60) Japan made instrument for thermal stability measurements.

Results and discussion

XRD analysis

Fig. 1 shows the crystalline properties of ZnO and rGO-ZnO nanocomposite as analyzed by the powder X-ray diffraction technique. Intense crystalline peak occurs at 26.0, which represents the hexagonal structure of the graphite and the peak shifts to 10.5 for Graphite Oxide due to the oxidation of graphite. At the time of
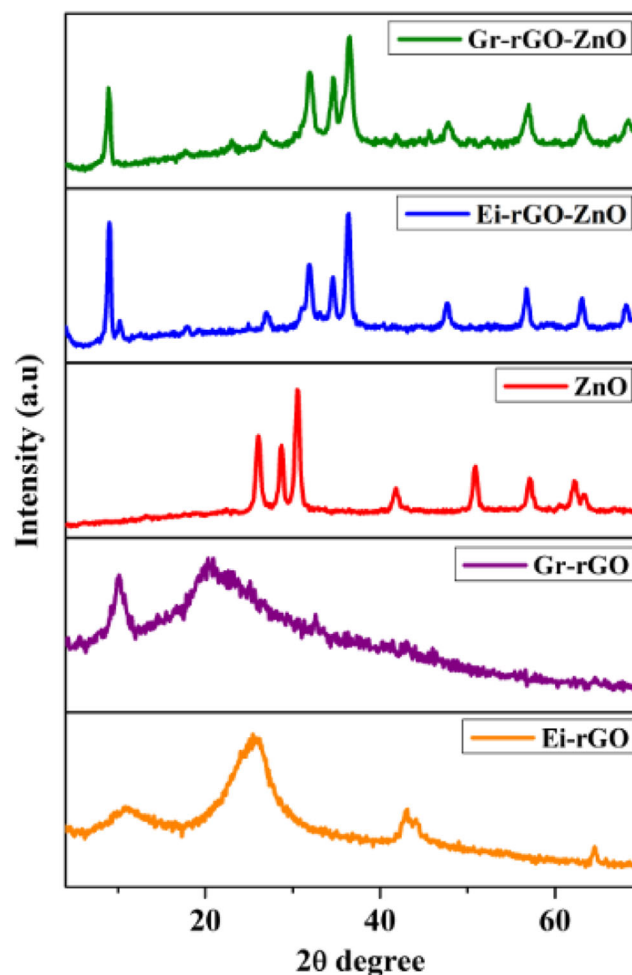

Fig. 1 XRD analysis: XRD for ZnO, Gr-rGO-ZnO, Ei-rGO-ZnO

oxidation the oxygen containing functional groups (C-OH, C-O-C, C-OOH) are intercalated with the graphite sheet and due to this intercalation, the d-spacing value is found to be expanded. After the reduction of Graphene Oxide by Grape and *Eichhornia crassipes* extract the peak shifts to 24.5, indicating the reducing property of Grape and *Eichhornia crassipes* extract [45]. In the XRD pattern of the ZnO nanoparticles (Fig. 1), the peaks at 31.7, 34.3,36.2, 47.4, 56.5, 62.7, 66.3, 67.8, 69.0, 72.4, 76.8, 81.2 and 89.4 correspond to (110), (002), (101), (102), (110), (103), (200), (112), (201), (004), (202), (104) and (203) crystalline planes of ZnO [46, 47]. All diffraction peaks in the XRD pattern of pure ZnO agree well with that of the hexagonal primitive ZnO phase (JCPDS 89–1397). A diffraction peak around $2\theta = 20$–$25°$ in the XRD pattern of the ZnO-rGO hybrid can be attributed to the (002) peak of the rGO.

HR-TEM analysis

Fig. 2a shows the TEM micro graphs of GO, in which the multiple sheeted structure of GO is clearly understood by the folding and wrinkle in the micrograph. In Fig. 2b and c the TEM micro graphs of rGO, the well exfoliated single sheeted structure is observed. The absence of wrinkle and folding suggest that the GO has been reduced to rGO by the removal of oxygen functionalities on its surface. The SAED pattern of GO shows multiple rings indicating the presence of multiple sheeted structure in GO. The SAED pattern of rGO structure shows sharp rings, indicating a short- range ordered rGO structure. The TEM micro graphs clearly bring out the reduction of GO to rGO by the natural reducing agents.
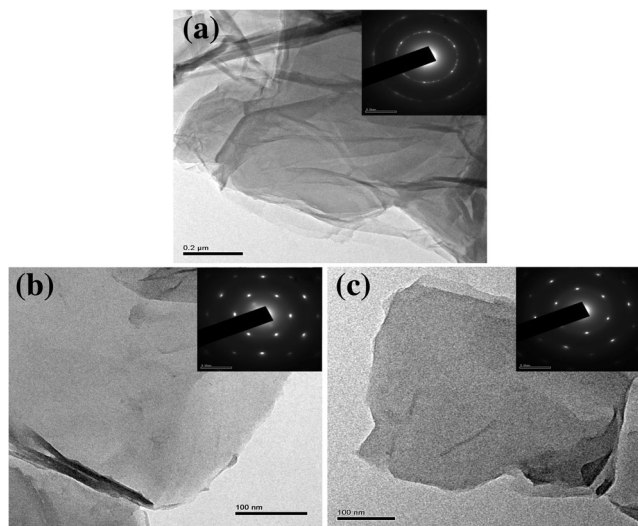

Fig. 2 High resolution-transmission electron microscope for (**a**) GO (**b**) Ei-rGO (**c**) Gr-rGO

SEM micrographs

The surface morphology of the prepared rGO and rGO based composite catalysts was investigated by SEM, it is shown in Fig. 3. SEM pictures of two different types of rGO prepared from two different natural reducing agents namely Grapes and *Eichhornia crassipes,* are shown in Fig. 2 (a) and (c) and they show the morphology of rGO. The synthesized rGO-ZnO composites (Fig. 2 (b) (d)) show a homogeneously distributed pattern. It is clearly observed that the surface of layered rGO nano sheet is packed densely by triangle shaped ZnO nanoparticles, which displays a good distribution of ZnO in the rGO. The morphological study clearly shows the formation of rGO-ZnO composites.

EDS was studied for understanding the elemental distribution. In Table 1 the presence of the element Zn on the rGO surface goes to confirm the formation of rGO-ZnO composites. From Table 1, it is seen that the elemental atomic % of Zn is around 3.85 and 3.99% on the surface of Gr-rGO and Ei-rGO nanocomposites respectively. The weight % of rGO-ZnO composites are 41.17, 27.43 and 31.40 for C, O and Zn respectively.

FT-IR spectra

The FTIR spectra of the GO, ZnO and rGO-ZnO nanocomposites are shown in Fig. 4. From the spectra the GO sample absorption band at 3400 cm-1 can be assigned to the O–H group stretching vibrations, the absorption peak at 1600 and 1500 cm-1can be assigned to C=O and C=C stretching of carboxylic and/or carbonyl moiety functional groups respectively. The peaks at 1000 and 900 cm-1are due to the stretching of C–OH and C–O groups respectively. The peaks around 2900 and 2800 cm^{-1}can be assigned to the asymmetric and symmetric vibrations of C–H band respectively. After the reduction of GO with the natural reducing agents Grape and *Eichhornia crassipes* extract, the intensity of the band for oxygen functional groups are found to decrease, which goes to prove that during the reduction there is a reduction in oxygen functionality in the GO [48]. In the ZnO spectra the strong absorption band in the range of <500 cm^{-1} corresponds to the vibrations of ZnO bonds. The FTIR spectrum of the rGO-ZnO nanocomposite shows a broad peak at 3400 cm^{-1}, which can be attributed to the O–H stretching vibration of the C–OH groups and water. In addition, the nanocomposite spectrum shows a strong absorption band in the range of <500 cm^{-1} which is due to the vibrations of the ZnO bonds, and which also goes to confirm the rGO-ZnO nanocomposite formation.
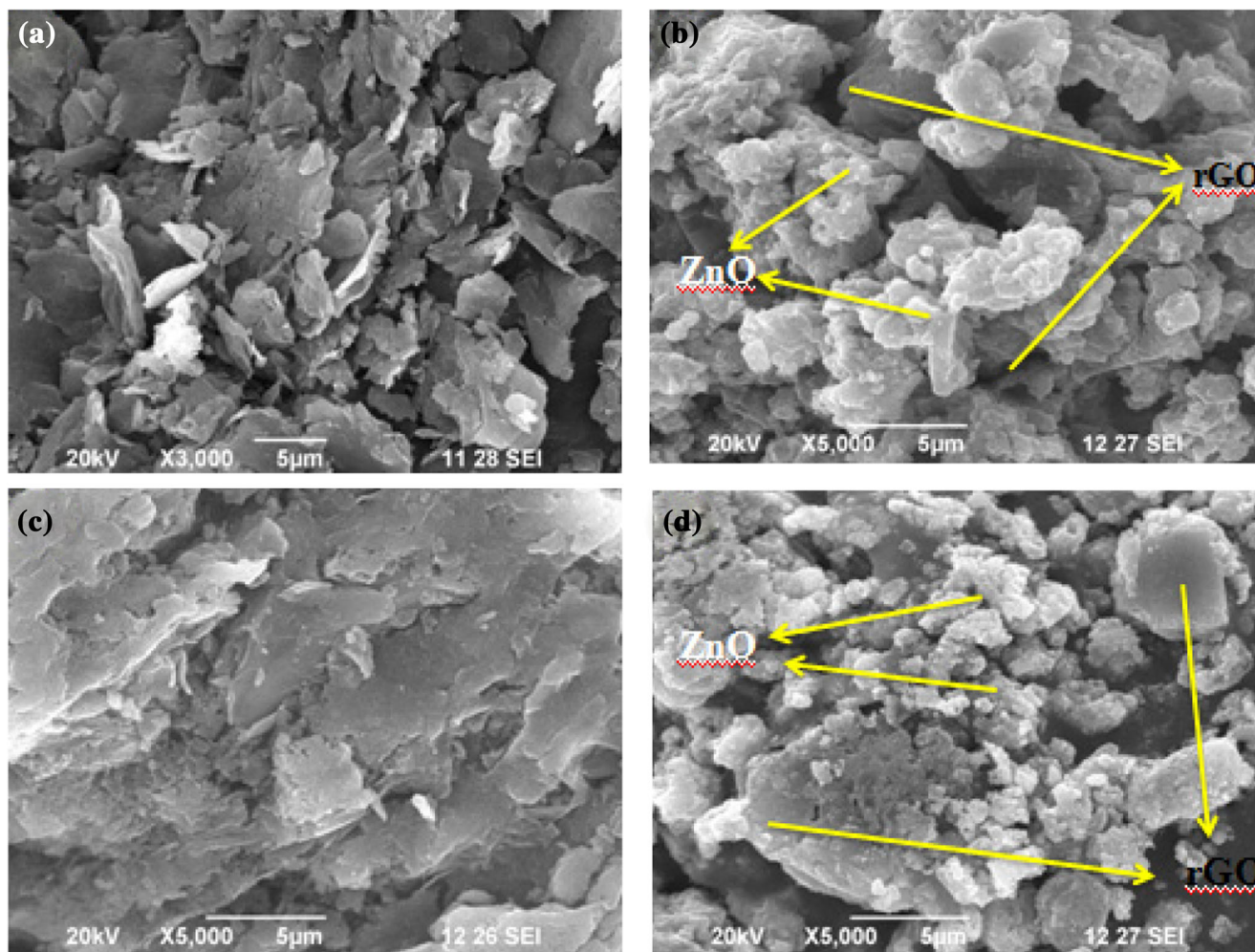
Fig. 3 SEM analysis: **a** SEM for Gr-rGO, (**b**) Gr-rGO-ZnO (**c**) SEM for Ei-rGO (**d**) Ei-rGO-ZnO

Optical imaging

The effectiveness of the formation of the rGO-ZnO nanocomposite can be seen in the optical imaging micrographs. Fig. 5a show the optical image of ZnO, which has a glittering appearance and Fig. 5b and c reveal the optical image of Gr-rGO and Ei-rGO and it clearly shows the presence of the sheeted form of rGO. The functionalized form of ZnO with rGO can be understood from the optical imaging picture (5d) and (4e). All these micrographs are useful for understanding the formation of rGO-ZnO nanocomposites.

Table 1   EDS value for Gr-rGO, Gr-rGO-ZnO, Ei-rGO, Ei-rGO-ZnO

	Gr-rGO	Gr-rGO-ZnO	Ei-rGO	Ei-rGO-ZnO
Carbon (Atomic %)	71.77	55.89	67.01	51.88
Oxygen (Atomic %)	28.23	40.26	32.99	44.13
Zinc (Atomic %)	–	3.85	–	3.99

Photoluminescence (PL) spectral studies

In this study, it is observed that the rGO-ZnO composite shows decreased emission intensity due to the inhibition of photogenerated carrier's recombination. ZnO has a high intensity peak and when it is treated with the two types of rGO (Grape and *Eichhornia crassipes*) it shows different types of intensity peaks. The Ei-rGO-ZnO composite shows a low intensity peak when compared with the Gr-rGO-ZnO composite. Therefore it is understood that the Ei-rGO-ZnO composite has more photogenerated carrier inhibition ability when compared to the Gr-rGO-ZnO composite, as shown in Fig. 6.

UV–vis spectra

The absorption spectra of graphene oxide, ZnO, reduced graphene oxide and rGO-ZnO composite are shown in Fig. 7. Graphene oxide and ZnO show a characteristic
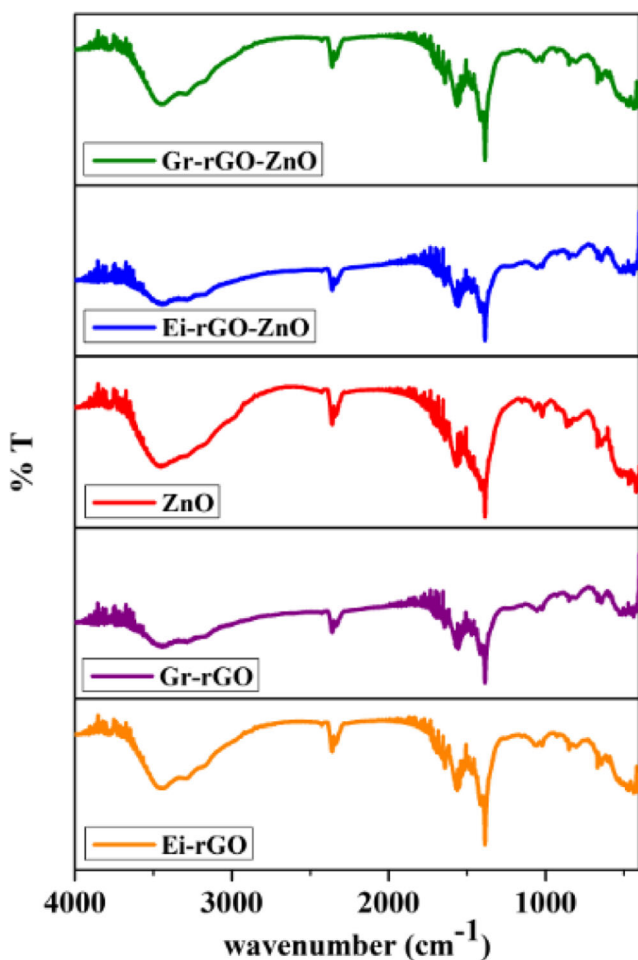
Fig. 4 FT-IR for Gr-rGO-ZnO, Ei-rGO-ZnO and ZnO

peak at 230 nm and 380 nm. The graphene oxide which is converted into two types of reduced graphene oxide by two different natural reducing agents namely Grape and *Eichhornia crassipes*, shows a characteristic peak at 270 nm. These reduced graphene oxides when treated with ZnO, show two characteristic peaks at 270 nm and 380 nm. UV-vis spectra is used to understand the photodegrading ability of the materials.

Proposed reaction mechanism for the reduction of graphene oxide by green extract

GO reacts with the reducing agents (grapes and *Eichhornia crassipes* leaf) present in the green extract Fig. 8. The alcohol group interacts with the epoxide group of GO. Due to the nuleophlic action of the O–H groups and removal of water, the epoxide group and phenolic groups of GO produce the intermediate. After 3 h of the reduction process, the rGO is formed along with the oxidized form.

Photocatalytic activity

Fig. 9 illustrates the photocatalytic activity of ZnO, Gr-rGO-ZnO and Ei-rGO-ZnO samples under visible light irradiation. It is witnessed that without any photocatalyst, there was no obvious degradation of RhB even after 120 min of visible-light irradiation. The band gap of ZnO and nanocomposites was estimated from the absorption edge of their respective
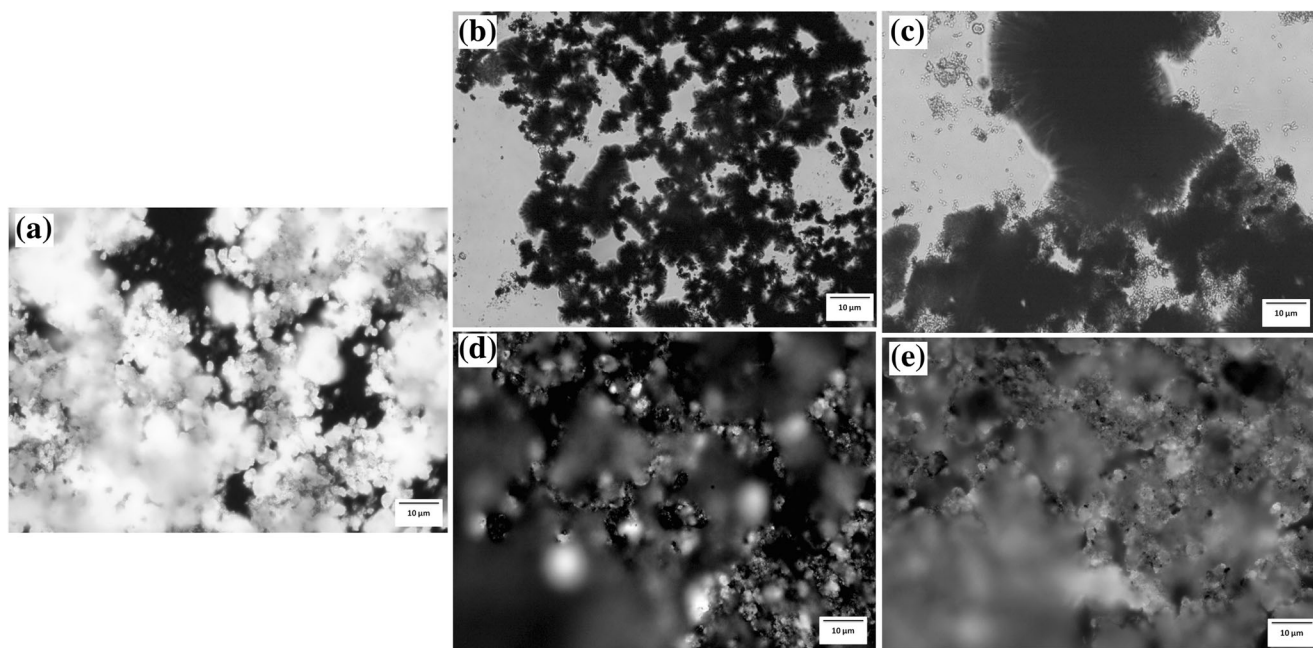

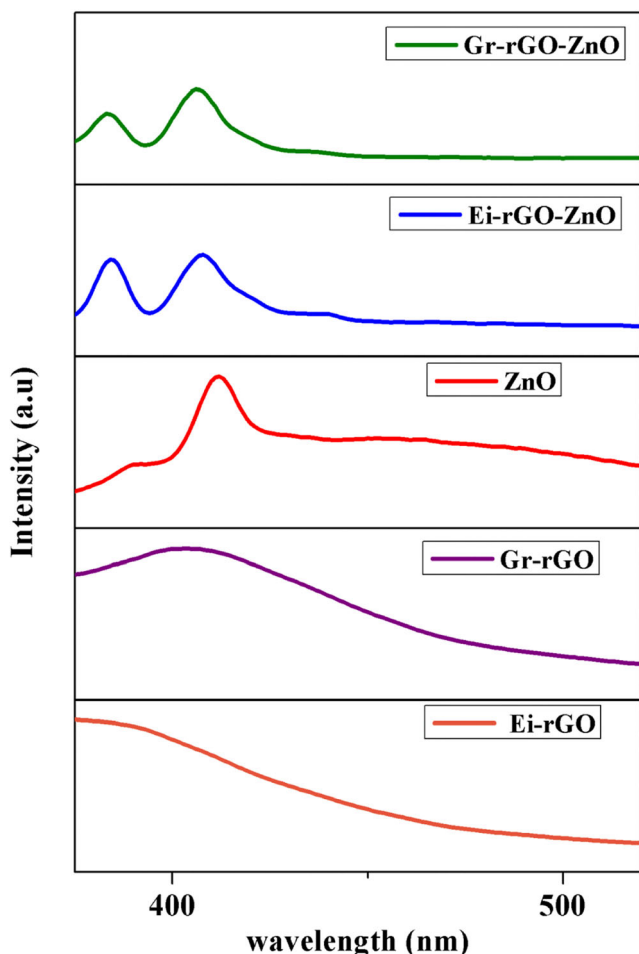Fig. 5 Optical Imaging (a) ZnO, (b) Gr-rGO, (c) Ei-rGO (d) Gr-rGO-ZnO (e) Ei-rGO-ZnO

Fig. 6 PL Spectra for Gr-rGO-ZnO, Ei-rGO-ZnO, ZnO

absorption spectra. The band gap of ZnO, Gr-rGO-ZnO and Ei-rGO-ZnO are estimated to be 3.05 eV, 3.02 eV, and 2.98 eV respectively. The observed red shift in the absorption edge of the nanocomposites compared to the bare ZnO indicates that the synthesized nanocomposites can be used as photocatalysts and the composites could absorb more photons (visible light)
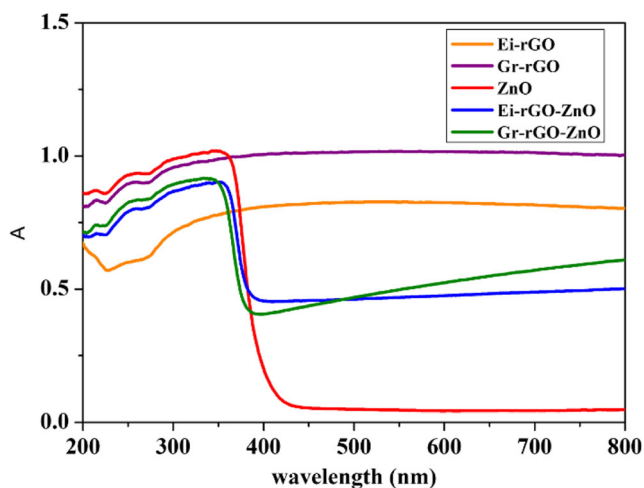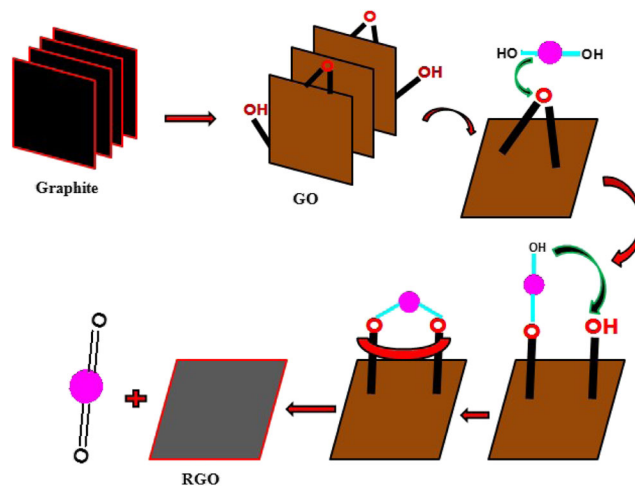

Fig. 7 UV Spectra for Gr-rGO-ZnO, Ei-rGO-ZnO, ZnO

Fig. 8 Plausible mechanism for the reduction of GO

than bare ZnO. Hence, the red shift observed in the absorption spectrum might enhance the photocatalytic efficiency. The removal rate of RhB for bare ZnO is 67%. The percentage degradation was enhanced to 97.5% when Ei-rGO-ZnO was added and a 70.0% degradation was achieved when the same amount of Gr-rGO-ZnO was added under similar conditions because of its higher band gap value compare to that of Ei-rGO-ZnO. The enhanced photocatalytic activity of Ei-rGO-ZnO composites could be attributed to the strong interaction with the ZnO and the defect sites available in Ei-rGO. After the irradiation of light, the electrons from the valence band of ZnO may be excited to its conduction band and consequently to the Ei-rGO. The molecules of MB can be transferred to the surface of the Ei-rGO-ZnO composites by means of p-p conjugation between the dye and the aromatic regions of Ei-rGO. The increase in number of holes initiates an oxidative pathway and therefore the adsorbed dye can be oxidized, as a result of which the photoactive radicals generated during the reaction produce CO_2, H_2O, and other intermediates, finally leading to the degradation of MB. This observation could be attributed to the increased active sites presence on the Ei-rGO-ZnO surface. Additionally, in the PL spectral studies it is observed that
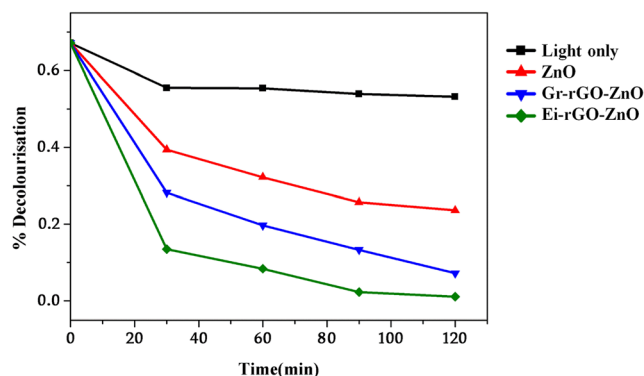

Fig. 9 Photocatalytic efficiency of Ei-rGO-ZnO, Gr-rGO-ZnO, ZnO and light in the degradation of RhB under visible light irradiation
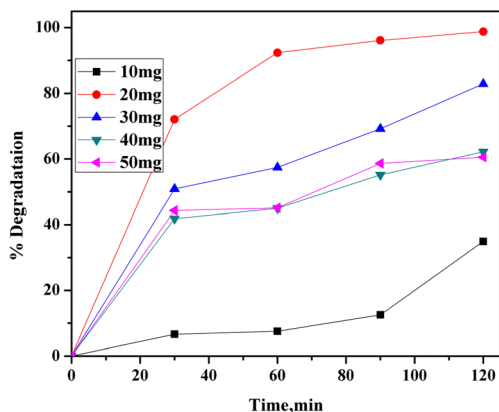
Fig. 10 The degradation of RhB dye solution using Ei-rGO-ZnO under visible light irradiation. RhB = [1×10^{-5} M], Temp = 35 ± 1 °C

Ei-rGO-ZnO has greater inhibition ability for the electron hole pair recombination, which will lead to enhanced photocatalytic activity. The inhibition of the recombination of photogenerated radicals leads to greater concentration of hydroxyl and superoxide radicals which facilitates high degradation efficiency. These results clearly show that the Ei-rGO-ZnO composite has a higher photocatalytic activity than the Gr-rGO-ZnO nanocomposite [49]. The pH variation showed that the degradation was efficient only at pH 7.

Effect of catalyst dosages

The photocatalyst degradation of RhB is strongly influenced by the amount of catalyst required for the photocatalytic reaction. As we have observed that Ei-rGO-ZnO showed a better photocatalytic activity towards the degradation of RhB, it is necessary to optimize the amount of catalyst required for a better degradation rate of RhB. Hence the effect of catalyst dosage on the photocatalytic degradation of RhB (1 X 10^{-5} M) was investigated. It can be seen in (Fig. 10) that the percentage degradation of RhB dye enhanced from 34.92 to 98.78 with increasing dosages of Ei-rGO-ZnO respectively
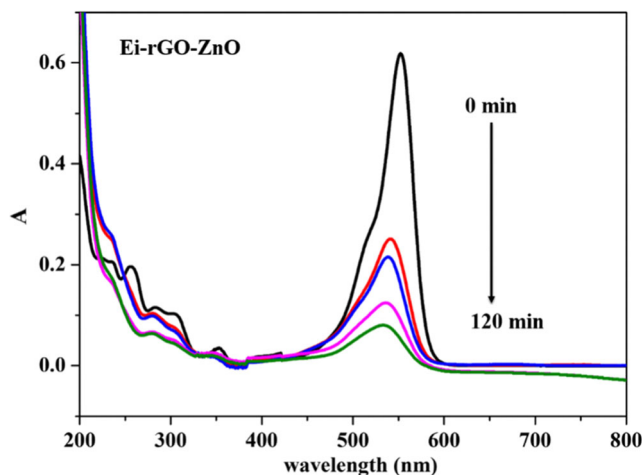

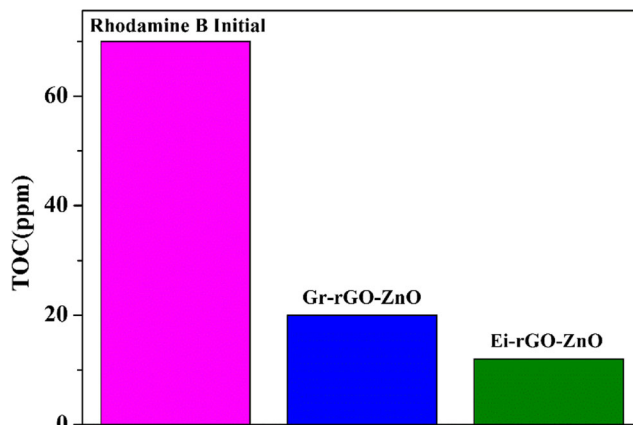**Fig. 11** Temporal changes of UV–VIS spectra of RhB

Fig. 12 Percentage degradation of TOC during photodegradation of RhB in presence of rGO-ZnO

from 10 mg to 20 mg which can be explained by the fact that the number of photo generated e^--h^+ pairs correspondingly increased with the increase of the catalyst dosage. However, further increase in the catalyst dosages from 20 mg to 50 mg led to a decline in the degradation percentage to 60.55 and 73.36 (50 mg) compared to a high value of 98.78 for 20 mg. Normally the increase in the amount of the catalyst increases the number of active sites which in turn increases the amount of. OH and $^-O_2$ radicals which would degrade RhB. But when the concentration of the catalyst increases above the optimum value, the percentage degradation decreases, due to the scattering effect of light by the catalyst particles. Sun et al. have reported that the excess catalyst prevented the penetration of the light, thus decreasing the primary oxidants in the photocatalytic system i.e. hydroxy radicals, which in turn decrease the percentage of degradation [46]. Also the excess amount of catalyst beyond the optimum concentration would agglomerate and render the catalyst surface unavailable for photon absorption resulting in decline in the photodegradation efficiency. Therefore, in this case, the optimal dosage of netted-shaped Ei-rGO-ZnO for RhB degradation is 20 mg/50 ml.

UV-vis absorption spectroscopy

Generally, photocatalytic degradation of RhB follows two mechanisms. i) attack of OH radical on the chromophore aromatic ring with hypochromic shift ii) successive de-ethylation from the aromatic ring leading to intermediate products with hypsochromic shift [50]. Fig. 11 exhibits the absorption spectra of RhB using rGO-ZnOa and the absorption peak at 554 nm decreased gradually with hypochromic shift and was nearly wiped out totally after 120 min of irradiation in the presence of both Gr-rGO-ZnO and Ei-rGO-ZnO nanocomposites, this confirms that degradation occurs through the aromatic ring opening of RhB dye for both the prepared catalysts. Further, no new absorption bands are seen in

Fig. 13 MS spectra of (**a**) RhB and (**b**) end products of the photocatalytic degradation of RhB
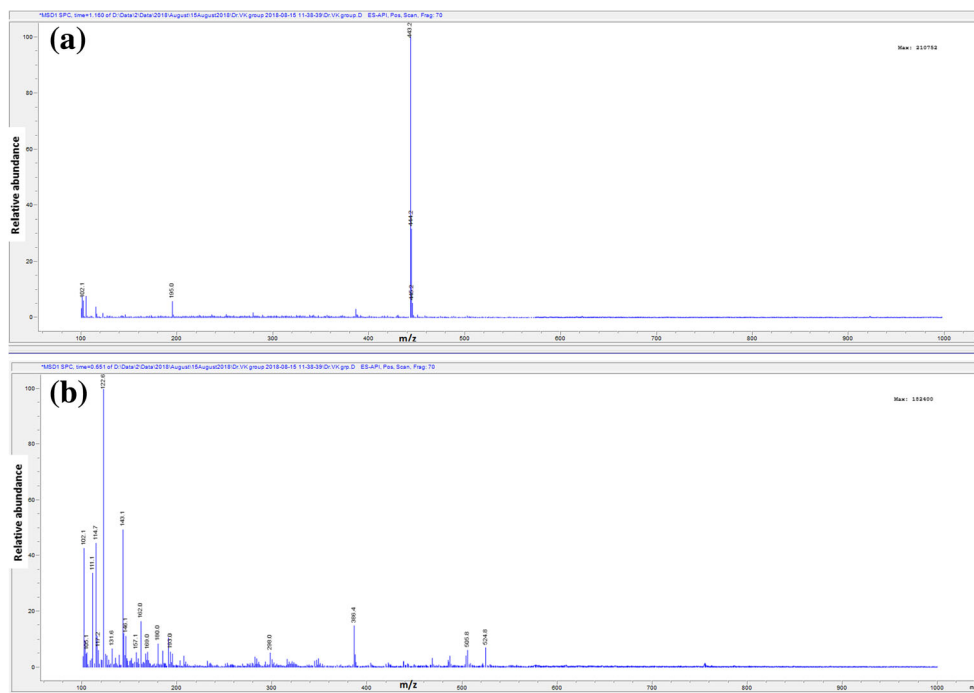
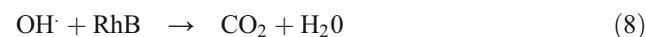the visible regions, which indicate the complete degradation of the RhB during the reaction.
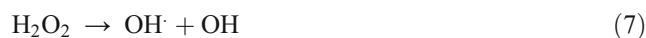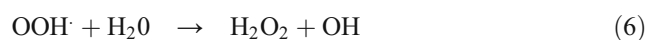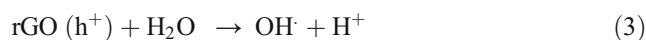
Total organic carbon (TOC)

During photodegradation of organic dyes some intermediates are formed that may be even more toxic than the initial compound. Therefore, TOC study was carried out to find the mineralization of RhB under visible light irradiation. Fig. 12 shows the initial dye TOC value and the value after degradation by both Gr-rGO-ZnO and Ei-rGO-ZnO composites under visible light irradiation. The results show that RhB dye was mineralized as indicated by the negligible TOC valueswhen compared with the initial dye concentration.

Mass spectra

The degradation of the RhB dye by photocatalysis was studies using the mass spectrophotometry, shows in Fig. 13. Some of the intermediated formed during the degradation were identified to be 9-(2-carboxyphenyl)-6-(diethylamino)-3H-xanthen-3-iminium (m/z-1 = 386 m/z), N-(6-(dimethylamino)-4H-xanthen-3(10aH)-ylidene)-N-ethylethanaminium (m/z-1 = 297), 2-(methoxycarbonyl) benzoic acid (m/z-1 = 180), 4-(ethyl(methyl)amino)benzene-1,2-diol (m/z-1 = 168), adipic acid (m/z-1 = 145), glutaric acid (m/z-1 = 131), Benzoic acid (m/z-1 = 121), Hexanoic acid (m/z-1 = 116), (E)-5,5-diaminopenta-2,4-dien-1-ol (m/z-1 = 113), (E)-pent-

3-ene-1,3-diol (m/z-1 = 101). Based on the intermediates formed, a plausible mechanism for the degradation is given in Fig. 14 [44, 51–54].

$$\text{rGO}-\text{ZnO} + \text{Visible light} \rightarrow \text{rGO (h}^+) + \text{ZnO (e}^-) \quad (2)$$

$$\text{rGO (h}^+) + H_2O \rightarrow OH^{\cdot} + H^+ \quad (3)$$

$$e^- + O_2 \rightarrow O_2^{\cdot-} \quad (4)$$

$$O_2^{\cdot-} + H_2O \rightarrow OOH^{\cdot} + OH^- \quad (5)$$

$$OOH^{\cdot} + H_2O \rightarrow H_2O_2 + OH \quad (6)$$

$$H_2O_2 \rightarrow OH^{\cdot} + OH \quad (7)$$

$$OH^{\cdot} + RhB \rightarrow CO_2 + H_2O \quad (8)$$

Plausible photodegradation mechanism

Generally, the improved photocatalytic activity of rGO-ZnO under visible light irradiation owing to its adsorption capacity, absorption of visible light capability and the suppression of recombination of
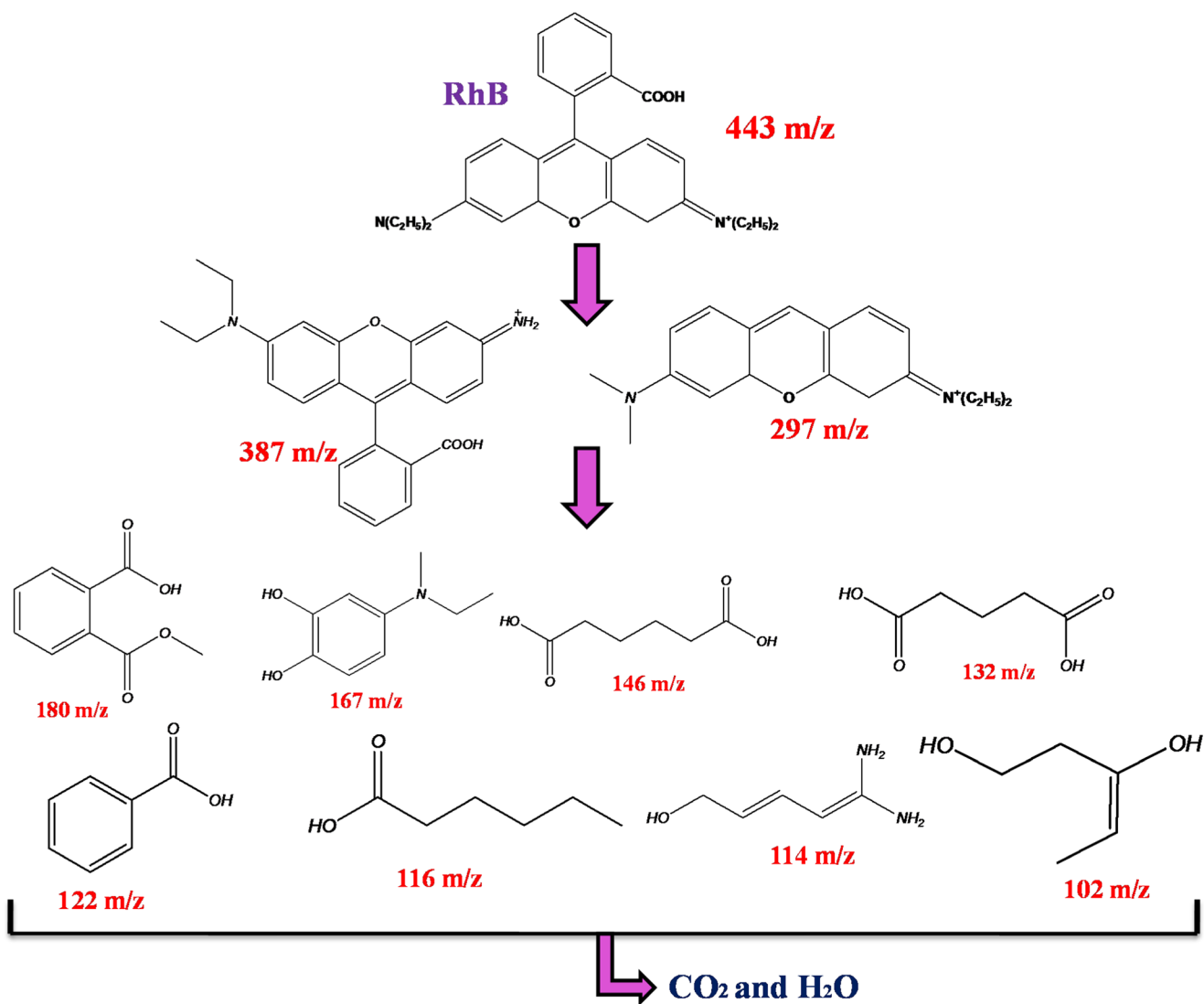
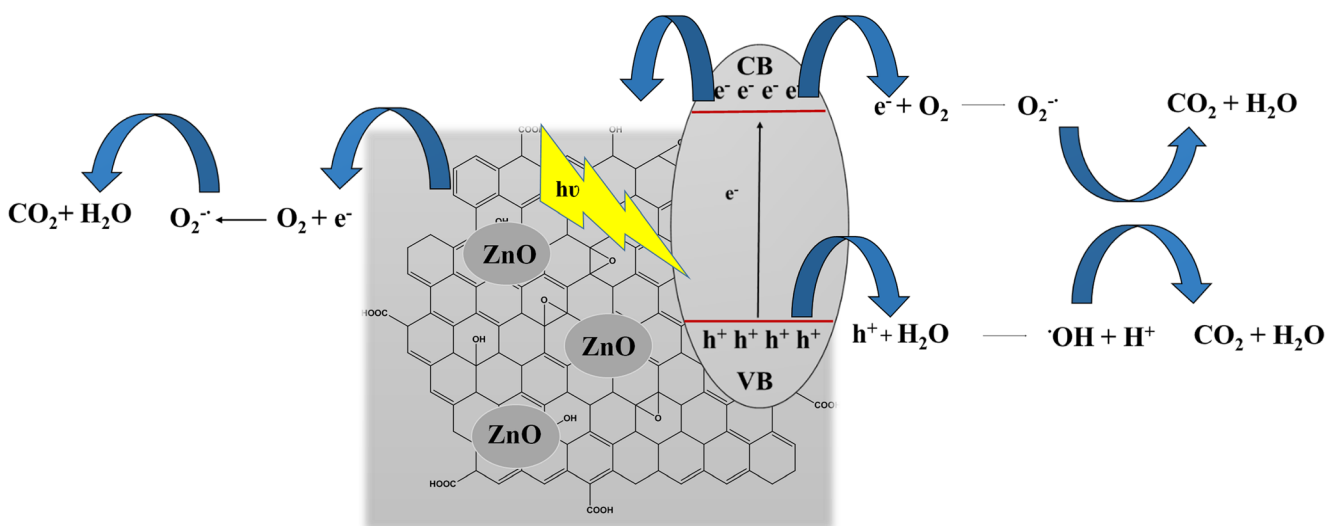Fig. 14 Plausible mechanism for the degradation of RhB dye

Fig. 15 Schematic representation of Rhodamine B dye degradation under visible light irradiation
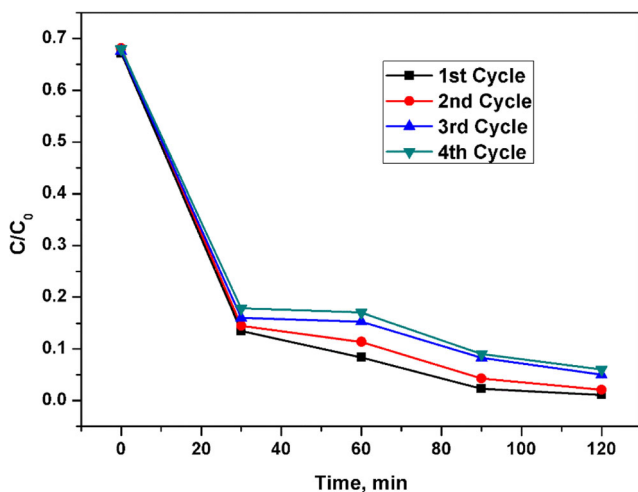
Fig. 16 Stability and reusability of Ei-rGO-ZnO photocatalyst in four successive cycles

electron hole pair. Fig. 15 shows the general mechanism of photodegradation of RhB under visible light irradiation. Initially, the excess of dyes are absorbed by the rGO-ZnO due to its large surface area. Then the electrons excited from RhB can be transferred to the rGO after the irradiation. Further, the electron transfer to ZnO conduction band, results in the reaction with the dissolved oxygen to give reactive oxygen species which can degrade the RhB. Meanwhile, the hole h^+ in the valence band of ZnO can oxidize the dye molecules directly. All these observations suggest that the photocatalytic activity of rGO-ZnO is enhanced due to the presence of rGO nanoparticles [55, 56].

Stability and reusability of photocatalyst

The stability and reusability of the photocatalyst was investigated by using the catalyst for four consecutive degradation reactions on RhB dye. All the four experiment carried out were under the same reaction conditions. After the completion of the degradation process in each reaction, the degraded solution was filtered and the left over catalyst was collected and it was dried under high vacuum. Then this collected catalyst was used for the next the degradation reaction of RhB dye. This experiment was repeated nearly four times with the same catalyst. From Fig. 16, it is observed that the catalytic efficiency of the used catalyst were 98%, 96%, 93% and 92% for the 1st, 2nd, 3rd and 4th cycle respectively. Therefore, it is evidence that the catalytic efficiency of the catalyst was almost retained even upto the fourth cycle. These results clearly show that the Ei-rGO-ZnO photocatalyst has good stability and reusability in the photocatalytic process [57].

Conclusion

In conclusion, Graphene oxide was synthesized by Hummers methods and it was converted into reduced graphene oxide using eco friendly reducing agents like Grapes and *Eichhornia crassipes*. These two rGO's were treated with ZnO to form the Gr-rGO-ZnO and Ei-rGO-ZnO nanocomposites. The photocatalytic degradation efficiency of Gr-rGO-ZnO and Ei-rGO-ZnO nanocomposite was studied on RhB dye under the visible light irradiation condition. Our results confirm that Ei-rGO-ZnO nanocomposite had higher degradation efficiency than the rGO-ZnO nanocomposite. These results can lead to improved development of photocatalytic degradation of organic dyes using cheap materials.

Compliance with ethical standards

References

1. Javaid Mughal M, Saeed R, Naeem M, Aleem Ahmed M, ArfaYasmien QS. Mansoor Iqbal Dye fixation and decolourization of vinyl sulphone reactive dyes by using dicyanidiamide fixer in the presence of ferric chloride. J Saudi Chem Soc. 2013;17:23.

2. Shahid M. Shahid-ul-Islam and Faqeer Mohammad. Recent advancements in natural dye applications: a review. J Clean Prod. 2013;53.

3. Kolani L, GbénonchiMawussi KS. Assessment of Organochlorine Pesticide Residues in Vegetable Samples from Some Agricultural Areas in Togo. American J Anal Chem. 2016;7:332.

4. Shirmardi M. Amir Hossein Mahvi, Alireza Mesdaghinia, Simin Nasseri, Ramin Nabizadeh. Adsorption of acid red18 dye from aqueous solution using single-wall carbon nanotubes: kinetic and equilibrium. Des Water Treat. 2013;51:6507–16.

5. Shirmardi M, Mahvi AH, Hashemzadeh B, Naeimabadi A, Hassani G, Niri MV. The adsorption of malachite green (MG) as a cationic dye onto functionalized multi walled carbon nanotubes. Korean. J Chem Eng. 2013;30:1603–8.

6. Ashrafi SD, Kamani H, Jaafari J, Mahvi AH. Experimental design and response surface modeling for optimization of fluoroquinolone removal from aqueous solution by NaOH-modified rice husk. Desalin Water Treat. 2015;57(35):16456–65.

7. Ashrafi SD, Rezaei S, Forootanfar H, Mahvi AH, Faramarzi MA. The enzymatic decolorization and detoxification of synthetic dyes by the laccase from a soil-isolated ascomycete, Paraconiothyrium

variabile. International Biodeterioration & Biodegradation. 2013;85:173–81.

8. Kamani H, Safari GH, Asgari G, Ashraf SD. Data on modeling of enzymatic elimination of direct red 81 using response surface methodology. Data Brief. 2018;18:80–6.

9. Mehrabian F, Kamani H, Safari GH, Asgari G, Ashraf SD. Direct Blue 71 removal from aqueous solution by laccase-mediated system; A dataset. Data in Brief. 2018;19:437–43.

10. Rahman F. The treatment of industrial effluents for the discharge of textile dyes using by techniques and adsorbents. J Textile Sci Eng. 2016;6:1.

11. Jain N, TanikaSethi NG. Review Paper on Various Techniques used in Effluent Treatment of Textile Industry. Int J Civil Eng. 2016;3:5.

12. Chandran D. Review of the textile industries waste water treatment methodologies. Int J Scientific & Eng Research. 2016;7:1.

13. Pang YL, Abdullah AZ. Current Status of Textile Industry Wastewater Management and Research Progress in Malaysia. In: A Review clean-soil, air, water, vol. 41; 2013. p. 751.

14. Dong S, Li J, Kim M-H, Park S-J, Gary Eden J, Guest JS, et al. Human health trade-offs in the disinfection of wastewater for landscape irrigation: microplasma ozonation *vs.* chlorination. Environ Sci Water Res Technol. 2017;3:106–18.

15. Ashrafi SD, Kamani H, Mahvi AH. The optimization study of direct red 81 and methylene blue adsorption on NaOH-modified rice husk. Desalin Water Treat. 2014;57(2):738–46.

16. Ashrafi SD, Kamani H, Soheil Arezomand H, Yousefi N, Mahvi AH. Optimization and modeling of process variables for adsorption of basic blue 41 on NaOH-modified rice husk using response surface methodology. Desalin Water Treat. 2015;57(30):14051–9.

17. Lubello C, Mori G, Munz G, Gori R. Powdered activated carbon and membrane bioreactors (MBRPAC) for tannery wastewater treatment: long term effect on biological and filtration process performances. Desalination. 2007;207:349–60.

18. Vatanpoura V, Sheydaeia M, Esmaeili M. Box-Behnken design as a systematic approach to inspect correlation between synthesis conditions and desalination performance of TFC RO membranes. Desalination. 2017;420:1.

19. Zhou Y, Huang M, Deng Q, Cai T. Combination and performance of forward osmosis and membrane distillation (FO-MD) for treatment of high salinity landfill leachate. Desalination. 2017;420:99.

20. Gahlot S, Sharma S, Electrodeionization VK. An efficient way for removal of fluoride from tap water using an aluminum form of Phosphomethylated resin. Ind Eng Chem Res. 2015;54:4664.

21. Narjes Jafari, Rouha Kasra-Kermanshahi, Mohammad Reza Soudi, Amir Hossein Mahvi and Sara Gharavi. Iranian Journal of Environmental Health Sciences & Engineering 2012; 9:33.

22. Rimoldi L, Meroni D, Falletta E, Pifferi V, Falciola L, Cappellettia G, et al. Emerging pollutant mixture mineralization by TiO_2 photocatalysts. The role of the water medium. Photochem Photobiol Sci. 2017;16:60.

23. Yang W, Liu H, Zhang M, Duan W, Liu B. A dual-functional UiO-66/TiO_2 composite for water treatment and CO_2 capture. RSC Adv. 2017;7:16232–7.

24. Karina Bustos-Ramírez, Carlos Eduardo Barrera-Díaz, Miguel De Icaza-Herrera, Ana Laura Martínez-Hernández, Reyna Natividad-Rangel and Carlos Velasco-Santos. Journal of Environmental Health Science & Engineering 2015; 13:33.

25. Dreyer DR, Park S, Bielawski CW, Ruoff RS. The chemistry of graphene oxide Chem. Soc Rev. 2010;39:228–40.

26. Novoselov KS, Geim AK, Morozov SV, Jiang D, Zhang Y, Dubonos S, et al. Electric field effect in atomically thin carbon films. Science. 2004;306:666–9.

27. M.D. Stoller, S. Park, Y. Zhu, J. An, R.S. Ruoff. Graphene-Based Ultracapacitors Nano Lett 2008; 8:3498–3502.

28. Liang M, Zhi L. Graphene-based electrode materials for rechargeable lithium batteries. J Mat Chem. 2009;19:5871–8.

29. Han MY, Oezyilmaz B, Zhang Y, Kim P. Energy band-gap engineering of graphene nanoribbons. Phys Rev Lett. 2007;98:206805.

30. Cheng C-E, Lin C-Y, Shan C-H, Tsai S-Y, Lin K-W. Platinum-graphene counter electrodes for dye-sensitized solar cells. J Appl Phys. 2013;014503:114.

31. Liu Y, Dong X, Chen P. Biological and chemical sensors based on graphene materials. Chem Soc Rev. 2012;41:2283.

32. Toh SY, Loh KS, Kamarudin SK, Daud WRW. Graphene production via electrochemical reduction of graphene oxide: synthesis and characterization. Chem Eng J. 2014;251:422–34.

33. Park S, An J, Potts JR, Velamakanni A, Murali S, Ruoff RS. Hydrazine-reduction of graphite- and graphene oxide. Carbon. 2011;49(9):3019–23.

34. Liu Y, Li Y, Yang Y, Wen Y. M. Wang reduction of graphene oxide by thiourea. J Nano Sci Nanotech. 2011;11(11):10082–6.

35. Shin HJ, Kim KK, Benayad A, Yoon SM, Park HK, Jung IS, et al. Efficient reduction of graphite oxide by sodium borohydride and its effect on electrical conductance. Adv. Funct. Mater. 2009;19(12): 1987–92.

36. E.C. Salas, Z. Sun, A. Lüttge, J.M. Tour. Reduction of Graphene Oxide *via* Bacterial Respiration ACS Nano. 2010;4(8): 4852–4856.

37. Zhang J, Yang H, Shen G, Cheng P, Zhang J, Guo S. Reduction of graphene oxide via L-ascorbic acid. Chem Commun. 2010;46: 1112–4.

38. Park S, Ruoff RS. Chemical methods for the production of graphenes. Nature Nanotech. 2009;4:217–24.

39. Ren PG, Yan DX, Ji X, Chen T, Li ZM. Temperature dependence of graphene oxide reduced by hydrazine hydrate. Nanotechnology. 2010;22:055705.

40. Si Y, Samulski T. Synthesis of water soluble graphene. Nano Lett. 2008;8(6):1679–82.

41. Narasimharao K, Venkata Ramana G, Sreedhar D, Vasudevarao V. Synthesis of graphene oxide by modified hummers method and hydrothermal synthesis of graphene-NiO Nano composite for supercapacitor application. J Material Sci Eng. 2016;5:6.

42. Gurunathan S, Han JW, Kim ES, Park JH, Kim J-H. Int J Nanomedicine. 2015;10:2951–69.

43. Chang DW, Jong-BeomBaek. Eco-friendly synthesis of graphene nanoplatelets. J Mater Chem A. 2016;4:15281.

44. Steplin Paul Selvin S, Ganesh Kumar A, Sarala L, Rajaram R, Sathiyan A, Princy Merlin J, et al. Photocatalytic degradation of rhodamine B using zinc oxide activated charcoal polyaniline nanocomposite and its survival assessment using aquatic animal model. ACS sustainable. Chem Eng. 2018;6:258−267.

45. Shirmardi M, Alavi N, Limae EC, Takdastana A. Amir Hossein Mahvi, Ali Akbar Babaei. Removal of atrazine as an organic micro-pollutant from aqueous solutions: a comparative study. Process Saf Environ Prot. 2016;103:23–35.

46. Moon IK, Lee J, Rodney S, Ruoff HL. Reduced graphene oxide by chemical graphitization. Nat Commun. 2010;1:73.

47. Venkata Ramana Posa, Viswadevarayalu Annavaram, Janardhan Reddy Koduru, Varada Reddy Ammireddy, and Adinarayana Reddy Somala. Graphene-ZnO nanocomposite for highly efficient photocatalytic degradation of methyl orange dye under solar light irradiation. Korean J Chem Eng 2016;2:456.

48. Ren P-G, Yan D-X, Ji X, Chen T, Li Z-M. Temperature dependence of graphene oxide reduced by hydrazine hydrate. Nanotech. 2011;055705:22.

49. Jabeen M, Ishaq M, Song W, Xu L, Maqsood I, Deng Q. UV-assisted photocatalytic synthesis of ZnO-reduced graphene oxide nanocomposites with enhanced photocatalytic performance in degradation of methylene blue. ECS Journal of Solid State Science and Technology. 2017;6(4):M36–43.

50. Chen C, Li X, Ma W, Zhao J, Hidaka H. Nick Serpone. J Phys Chem B. 2002;106:318–24.

51. He Z, Sun C, Yang S, Ding Y, He H, Wang Z. Photocatalytic degradation of rhodamine B by Bi2WO6 with electron accepting agent under microwave irradiation: mechanism and pathway. J Hazard Mater. 2009;162(2):1477–86.

52. Yu K, Yang S, He H, Sun C, Gu C, Ju Y. Visible lightdriven photocatalytic degradation of rhodamine B over NaBiO3: pathways and mechanism. J Phys Chem A. 2009;113(37):10024–32.

53. He Z, Yang S, Ju Y, Sun C. Microwave photocatalytic degradation of rhodamine B using TiO2 supported on activated carbon: mechanism implication. J Environ Sci. 2009;21(2):268–72.

54. Xu H, Li H, Sun G, Xia J, Wu C, Ye Z, et al. Photocatalytic activity of La2O3-modified silver vanadates catalyst for rhodamine B dye degradation under visible light irradiation. Chem Eng J. 2010;160(1):33–41.

55. Nipane SV, Korake PV, Gokavi GS. Facile electrochemical assisted synthesis of ZnO/graphene nanosheets with enhanced photocatalytic activity. Ceram Int. 2015;41:4549.

56. Zhang C, Zhang J, Su Y, Xu M, Yang Z, Zhang Y. ZnO nanowire/reduced graphene oxide nanocomposites for significantly enhanced photocatalytic degradation of rhodamine 6G. Physica E: Low-dimensional Systems and Nanostructures. 2014;56:251.

57. Steplin Paul Selvin S, Radhika N, Oimang Borang I, Sharmila Lydia J. Princy Merlin. Visible light driven photodegradation of rhodamine B using cysteine capped ZnO/GO nanocomposite as photocatalyst. J Mater Sci Mater Electron. 2017;28:6722–30.